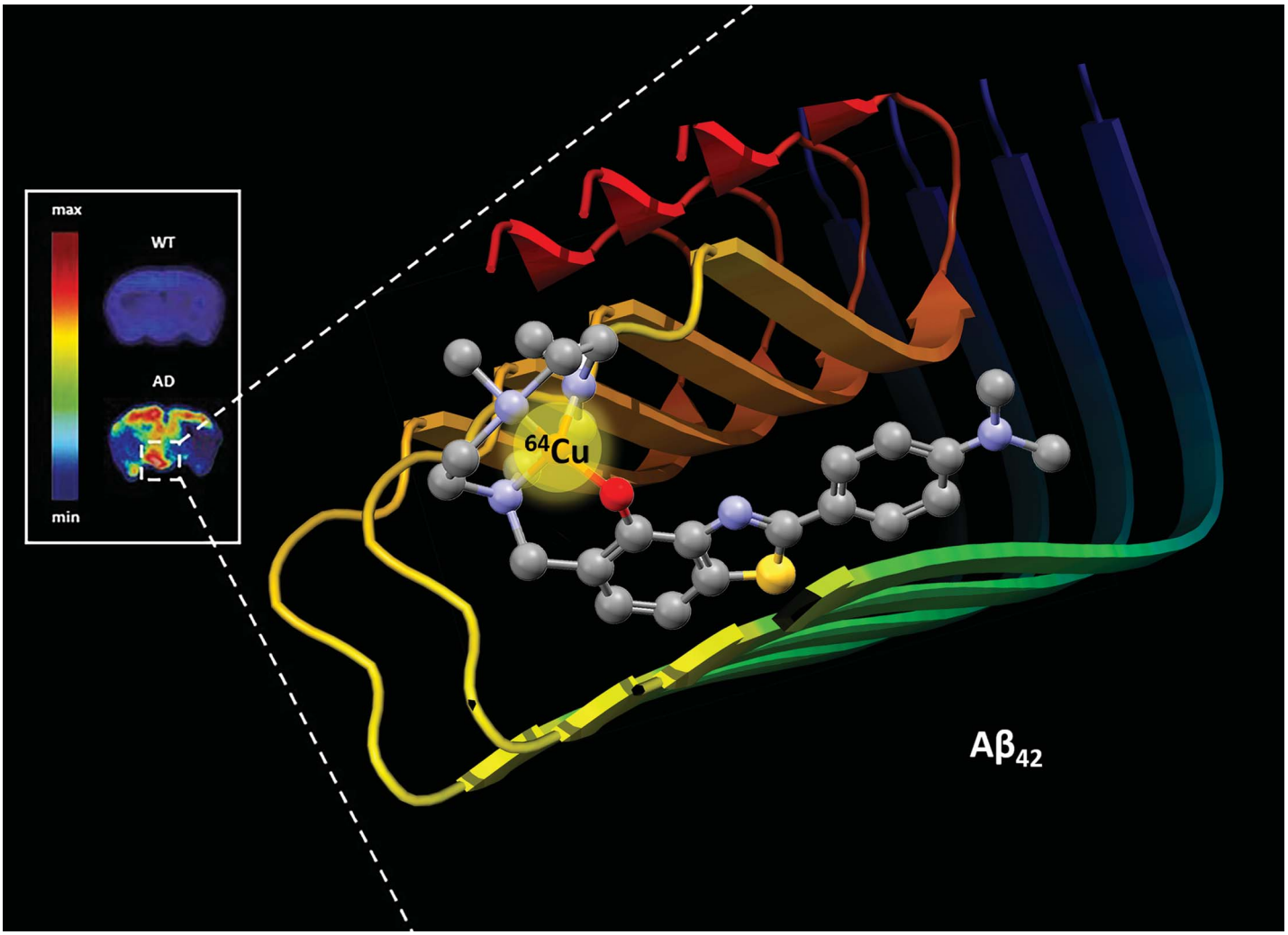

Showcasing research from Professor Liviu M. Mirica's laboratory, Department of Chemistry, University of Illinois at Urbana-Champaign, Urbana, Illinois 61801, USA.

Metal-chelating benzothiazole multifunctional compounds for the modulation and ^{64}Cu PET imaging of Aβ aggregation

Reported herein are a series of multifunctional compounds (MFCs) with appreciable affinity for amyloid aggregates that can be potentially used for both the modulation of amyloid β (Aβ) peptide aggregation and its toxicity, as well as for positron emission tomography (PET) imaging of Aβ aggregates by pre-chelation of these MFCs with the longer-lived ^{64}Cu radioisotope. By evaluating the various properties of these MFCs, valuable structure-activity relationships were obtained that should aid the design of improved therapeutic and diagnostic agents for AD.

As featured in:

See Buck E. Rogers, Liviu M. Mirica *et al.*, *Chem. Sci.*, 2020, **11**, 7789.

ROYAL SOCIETY OF CHEMISTRY

rsc.li/chemical-science

Registered charity number: 207890

Chemical Science

ROYAL SOCIETY OF CHEMISTRY

EDGE ARTICLE

View Article Online
View Journal | View Issue

Cite this: *Chem. Sci.*, 2020, **11**, 7789

All publication charges for this article have been paid for by the Royal Society of Chemistry

Metal-chelating benzothiazole multifunctional compounds for the modulation and ^{64}Cu PET imaging of Aβ aggregation†

Yiran Huang,[a] Hong-Jun Cho,[a] Nilantha Bandara,[b] Liang Sun,[a] Diana Tran,[b] Buck E. Rogers*[b] and Liviu M. Mirica*[ac]

While Alzheimer's Disease (AD) is the most common neurodegenerative disease, there is still a dearth of efficient therapeutic and diagnostic agents for this disorder. Reported herein are a series of new multifunctional compounds (MFCs) with appreciable affinity for amyloid aggregates that can be potentially used for both the modulation of Aβ aggregation and its toxicity, as well as positron emission tomography (PET) imaging of Aβ aggregates. Firstly, among the six compounds tested **HYR-16** is shown to be capable to reroute the toxic Cu-mediated Aβ oligomerization into the formation of less toxic amyloid fibrils. In addition, **HYR-16** can also alleviate the formation of reactive oxygen species (ROS) caused by Cu^{2+} ions through Fenton-like reactions. Secondly, these MFCs can be easily converted to PET imaging agents by pre-chelation with the ^{64}Cu radioisotope, and the Cu complexes of **HYR-4** and **HYR-17** exhibit good fluorescent staining and radiolabeling of amyloid plaques both *in vitro* and *ex vivo*. Importantly, the ^{64}Cu-labeled **HYR-17** is shown to have a significant brain uptake of up to 0.99 ± 0.04 % ID per g. Overall, by evaluating the various properties of these MFCs valuable structure–activity relationships were obtained that should aid the design of improved therapeutic and diagnostic agents for AD.

Received 12th May 2020
Accepted 7th July 2020

DOI: 10.1039/d0sc02641g

rsc.li/chemical-science

Introduction

Alzheimer's disease (AD) is the most common neurodegenerative disease, associated with loss of memory and cognitive decline.[1] An estimated 5.8 million Americans of all ages are living with Alzheimer's dementia currently.[2] The presence of amyloid plaques and neurofibrillary tangles in the brain is the hallmark of AD.[3] Amyloid β (Aβ) peptides, the main component of amyloid plaques,[4–7] are formed from the cleavage of amyloid precursor protein (APP) by β- and γ-secretases. The main alloforms of Aβ are $Aβ_{40}$ and $Aβ_{42}$, containing 40 and 42 amino acids, respectively.[8] Even though $Aβ_{40}$ is present in the deposits in larger amounts, $Aβ_{42}$ exhibits higher neurotoxicity and aggregates more easily.[9–12] In the past two decades, soluble Aβ oligomers have been found to be the most toxic form among all Aβ species[13–19] through their interactions with membrane and synaptic receptors[18,20] that influence intracellular systems[21] and affect neurotransmission,[22,23] leading to neurodegeneration.

In addition, the amyloid deposits contain uncommonly high concentrations of metal ions such as Fe^{2+}, Cu^{2+} and Zn^{2+},[24,25] and it has been found that these metal ions promote the formation of neurotoxic Aβ aggregates.[26–29] Cu and Fe ions can also cause the formation of reactive oxygen species (ROS), which exacerbates Aβ toxicity.[25,30–32] Previously, we have reported that Cu^{2+} ions can slow down Aβ fibrillization and stabilize Aβ oligomers,[33,34] and thus small molecules that can inhibit the interaction between metal ions and Aβ peptides, can be used as potential therapeutic compounds for AD.[35–38]

Moreover, the development of novel diagnostic agents is essential for the prevention and treatment of AD. Recently, several positron emission tomography (PET) compounds have been approved by FDA and can be used to visualize amyloid plaques in AD patients. However, these radiolabeled agents are employing short-lived radionuclides, such as ^{11}C and ^{18}F ($t_{1/2}$ = 20.4 min and 109.8 min,[39–45] respectively), thus limiting their widespread use. Thus, the development of longer-lived radiolabeled compounds is essential for further expanding the use of PET imaging in healthcare, and diagnostic agents employing longer-lived radionuclides such as ^{64}Cu ($t_{1/2}$ = 12.7 h, $β^+$ = 17%, $β^-$ = 39%, EC = 43%, E_{max} = 0.656 MeV) are viewed as optimal PET imaging agents.[46,47]

[a]*Department of Chemistry, University of Illinois at Urbana-Champaign, 600 S. Mathews Avenue, Urbana, Illinois 61801, USA. E-mail: mirica@illinois.edu*

[b]*Department of Radiation Oncology, Washington University School of Medicine, St. Louis, Missouri 63108, USA*

[c]*Hope Center for Neurological Disorders, Washington University School of Medicine, St. Louis, MO 63110, USA*

† Electronic supplementary information (ESI) available: Experimental section and Fig. S1–S8. See DOI: 10.1039/d0sc02641g

We have previously reported first-generation multifunctional compounds (MFCs) that contain Aβ binding and metal chelating fragments[33,48] and these MFCs were found to have the ability to modulate the aggregation of $A\beta_{42}$ species, although some led to the formation of neurotoxic soluble $A\beta_{42}$ oligomers.[33,48] Moreover, some MFCs could be converted into PET imaging agents through pre-chelation with ^{64}Cu and have with MFCs, PET imaging agents could be obtained for the diagnosis of Alzheimer's disease.[49,50] Herein, we report a series of second-generation multifunctional compounds (MFCs) containing metal-binding and Aβ-interacting fragments that also exhibit additional key properties (Fig. 1). In contrast to the first-generation MFCs, which were shown to promote the formation of neurotoxic oligomeric Aβ species,[33,48] these MFCs are capable of re-routing the neurotoxic metal-stabilized Aβ oligomers into less toxic aggregates, while also decreasing the formation of ROS. Moreover, these MFCs can be easily converted into PET imaging agents by chelation with the ^{64}Cu radionuclide, and *ex vivo* labeling studies using AD mouse brain sections reveal that the MFCs and their Cu complexes can clearly label the amyloid plaques. In addition, biodistribution studies show that the ^{64}Cu-radiolabeled compounds cross the blood–brain barrier (BBB) efficiently and thus should be able to act as potential therapeutic or imaging agents *in vivo*. Finally, structure–activity relationship (SAR) studies suggest that the presence of a monomethylamine group leads to increased specificity for binding to the Aβ aggregates, while the introduction of a pyridyl group is essential for modulating the neurotoxicity of metal–Aβ species. Most importantly, repositioning of the hydroxyl group and the metal-chelating azamacrocycle on the benzothiazole ring in **HYR-17** has a dramatic effect on improving the brain uptake of the corresponding ^{64}Cu complex, which could be a useful design approach for the development of improved PET imaging agents.

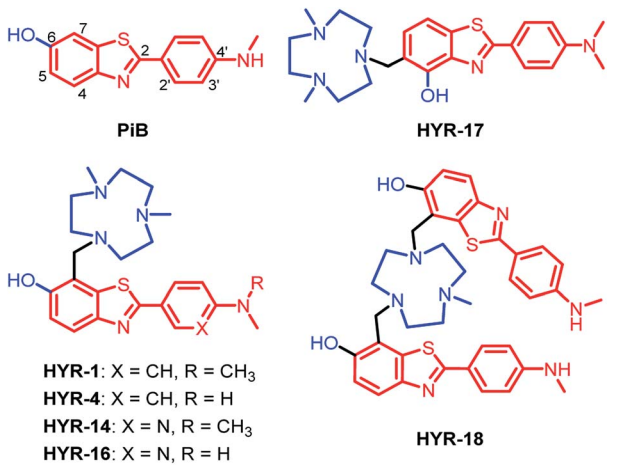

Fig. 1 Structures of Pittsburgh compound B (PiB) and the developed multifunctional compounds (MFCs) HYR-1, -4, -14, -16, -17 and -18. The metal-binding and Aβ-interacting fragments are shown in blue and red, respectively. The numbering of the different positions on the aromatic rings is shown only for the first structure.

Results and discussion

Design, synthesis and characterization of MFCs

Following up on our previous results, we set out to develop second-generation MFCs aimed to better alleviate the metal-induced Aβ toxicity, while also obtaining valuable structure–activity relationships (SAR) that should give us insight into the design of improved therapeutic and imaging agents for AD.

Previously, 2-aryl-benzothiazole derivatives have been found to have appreciable Aβ binding affinity and fluorescence properties,[33,48] and thus we continued to use such molecular frameworks. Inspired by the structure of Pittsburgh compound B (**PiB**, Fig. 1), a widely-used amyloid-binding compound with high Aβ binding affinity,[39] we introduced a hydroxyl group in the 6-position of the benzothiazole aromatic ring (Fig. 1). In addition, dimethylamino and monomethylamino groups were introduced at the 4′ position of the phenyl ring, since such functional groups are present in many Aβ binding compounds such as Thioflavin T (ThT) and Florbetapir.[43,51] Then, we have introduced a 1,4-dimethyl-1,4,7-triazacyclononane (tacn) metal-chelating group attached to the benzothiazole aromatic ring in order to generate a MFC that can modulate the metal–Aβ interactions. Importantly, previous studies have shown that the tacn-phenolate metal-chelating fragment can bind more tightly to Cu *versus* other metal ions such as Zn and Fe.[52–54] Accordingly, **HYR-1** and **HYR-4** were developed, and we have also designed **HYR-14** and **HYR-16** as 3′-pyridyl analogues in order to probe the effect of a hydrogen-bond acceptor pyridyl group *vs.* a phenyl group.[43,51] Moreover, it was previously found that a **PiB** derivative with a hydroxyl group in the 4-position of benzothiazole framework performed similarly as **PiB** in Aβ binding and bio-distribution studies,[55] and thus we have designed **HYR-17**, which contains a 4-hydroxyl substituent and has the tacn azamacrocycle connected to the 5 position of the benzothiazole ring (Fig. 1). Finally, the MFC **HYR-18** that contains two 2-aryl-benzothiazole fragments attached to one tacn azamacrocycle was also synthesized, in order to probe whether additional Aβ binding fragments will improve the affinity for Aβ aggregates.

The synthesis of the MFCs **HYR-1**, **-4**, **-14**, **-16**, **-17** and **-18** follows a stepwise sequence of steps that typically includes an oxidative cyclization step between a 2-amino-methoxybenzenethiol derivative and a benzaldehyde or benzoic acid derivative to generate the 2-aryl-benzothiazole fragments (Scheme 1). In cases where the 2-amino-methoxybenzothiazole precursor was readily available, hydrolysis under basic conditions afforded the 2-amino-methoxybenzenethiol starting materials, while for the pyridyl derivatives 2-amino-5-(trifluoromethyl)pyridine was employed in the oxidative cyclization reaction. Reduction of the nitro group to the aniline derivative using tin(II) chloride (if needed) and subsequent *N*-monomethylation using paraformaldehyde and sodium borohydride or *N*-dimethylation using paraformaldehyde and sodium cyanoborohydride generated the 2-(4′-aniline-aryl)-benzothiazole derivatives. Deprotection of the methoxy group using boron tribromide afforded the hydroxyl-benzothiazole derivatives, while the last synthetic step for all

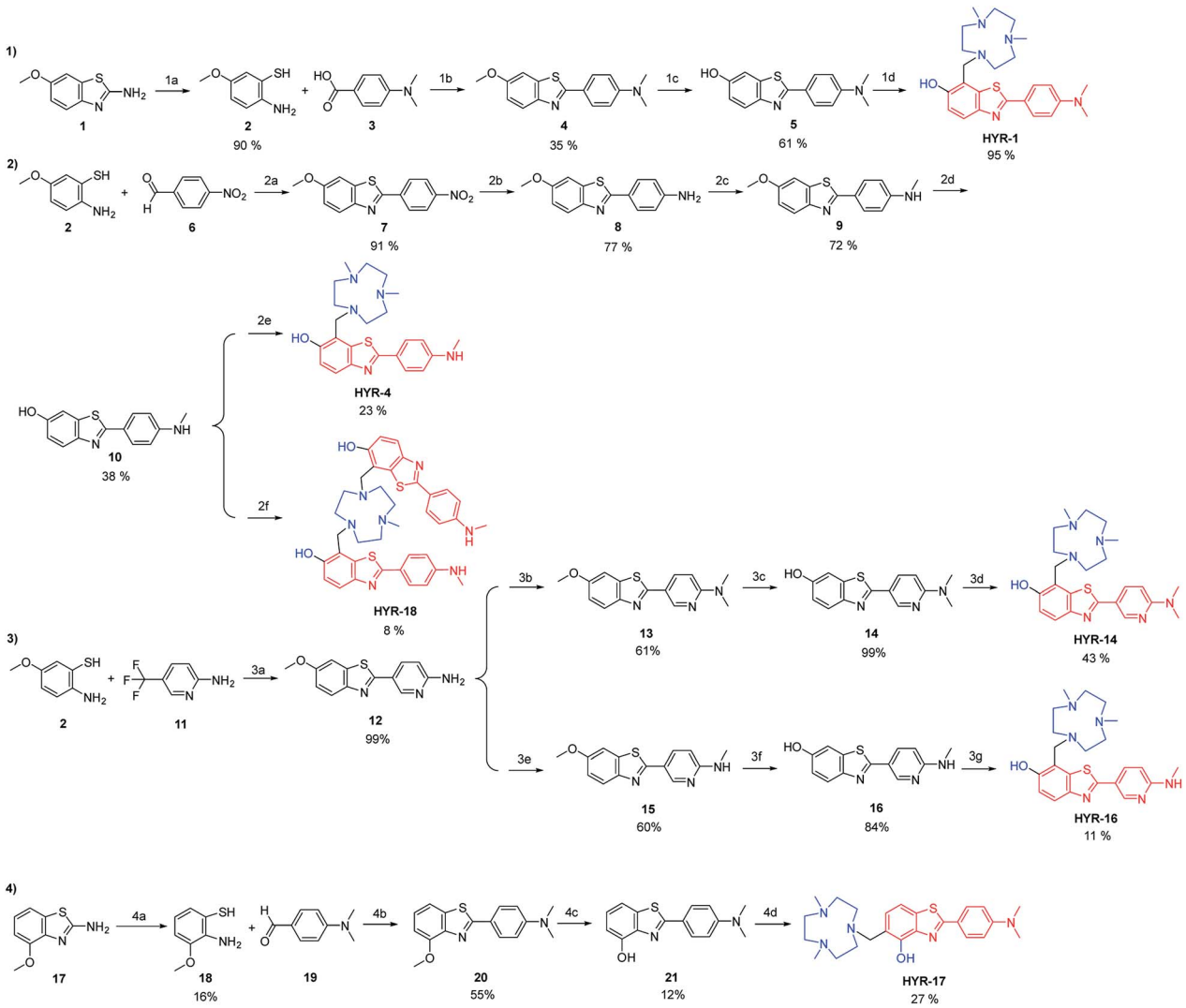

Scheme 1 Synthesis of the investigated MFCs **HYR-1**, **-4**, **-14**, **-16**, **-17** and **-18**. The metal-binding and Aβ-interacting fragments are shown in blue and red, respectively. Reagents and conditions: (1a) KOH, H_2O, ethylene glycol, reflux, 48 h; (1b) DMSO, 170 °C, 30 min; (1c) BBr_3, DCM, rt, 24 h; (1d) Me_2HTACN, $(CH_2O)_n$, MeCN, reflux, 24 h; (2a) DMSO, 125 °C, overnight; (2b) $SnCl_2$, EtOH, conc. HCl, reflux, 3 h; (2c) (i) $(CH_2O)_n$, NaOMe, MeOH, reflux, 2 h; (ii) $NaBH_4$, 0 °C to rt, 1 h; (2d) BBr_3, DCM, rt, 24 h; (2e) Me_2HTACN, $(CH_2O)_n$, MeCN, reflux, 24 h; (2f) MeH_2TACN, $(CH_2O)_n$, MeCN, reflux, 24 h; (3a) NaOH (1 M), 90 °C, 3 h; (3b) $(CH_2O)_n$, $NaBH_3CN$, acetic acid, rt, overnight; (3c) BBr_3, DCM, rt, 24 h; (3d) Me_2HTACN, $(CH_2O)_n$, MeCN, reflux, 24 h; (3e) (i) $(CH_2O)_n$, NaOMe, MeOH, reflux, 2 h; (ii) $NaBH_4$, reflux, 1 h; (3f) BBr_3, DCM, rt, 24 h; (3g) Me_2HTACN, $(CH_2O)_n$, MeCN, reflux, 24 h; (4a) KOH, H_2O, ethylene glycol, reflux, 48 h; (4b) DMSO, 125 °C, 30 min; (4c) BBr_3, DCM, rt, 24 h; (4d) Me_2HTACN, $(CH_2O)_n$, MeCN, reflux, 24 h.

compounds is the Mannich reaction with paraformaldehyde and 2,4-dimethyl-1,4,7-triazacyclononane under reflux to generate the targeted MFCs (Scheme 1).

ThT fluorescence competition assays

In order to measure the binding affinity of MFCs toward amyloid fibrils, ThT fluorescence competition assays were performed. The $A\beta_{40}$ peptide was used in these experiments, since it is known that $A\beta_{40}$ forms well-defined amyloid fibrils.[56,57] Excitingly, **HYR-1** and **HYR-4** exhibit nanomolar affinities for the $A\beta_{40}$ fibrils with K_i values of 11 ± 7 nM and 85 ± 9 nM, respectively, indicating that the MFCs can replace ThT efficiently and bind tightly to the $A\beta_{40}$ fibrils (Fig. 2). However, for the other MFCs it was difficult to obtain reproducible K_i values, likely due to the larger structural differences between these MFCs and ThT and thus the inability to compete with ThT for

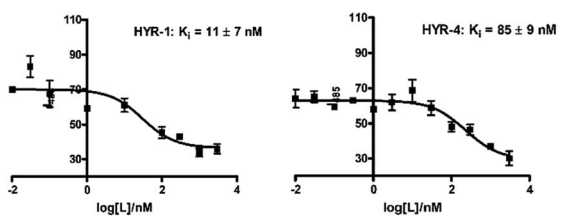

Fig. 2 ThT fluorescence competition assays for MFCs **HYR-1** and **HYR-4** with ThT-bound $A\beta_{40}$ fibrils ([Aβ] = 5 μM, [ThT] = 2 μM).

the same binding site(s) on the amyloid fibrils and that not lead to an appreciable decrease in ThT fluorescence. In addition, we consider that probing the affinity of the MFCs toward native amyloid plaques by performing *ex vivo* binding studies with transgenic AD mice brain sections should provide more physiologically relevant results and also rule out any non-specific binding (see below).

Fluorescence imaging of amyloid plaques in 5×FAD mice brain sections

Brain sections collected from 8 month-old 5×FAD transgenic mice were employed in these *ex vivo* Aβ binding studies. The transgenic 5×FAD mice overexpress mutant forms of the amyloid precursor protein (APP) and presenilin 1, develop amyloid plaque deposits at an younger age, and show progressive cognitive impairment similar to that found in AD in humans.[58]

Interestingly, incubation of the 5×FAD mouse brain sections with the different MFCs for 1 hour reveals significant fluorescent staining of the amyloid plaques, as confirmed by co-staining with Congo Red (CR), a well-known amyloid-binding fluorescent dye (Fig. 3). Among the MFCs, **HYR-1**, **-4**, **-17**, and **-18** show significant amyloid staining at low concentration (25 μM), suggesting an appreciable Aβ binding affinity. The most specific amyloid-binding MFCs are **HYR-4** and **HYR-18** (and **HYR-17** to a slightly lesser extent), which bind to the dense core of the amyloid plaques and thus show the best colocalization with CR. By contrast, **HYR-1** seems to label other endogenous proteins, both in AD and WT brain sections (Fig. 3 and S5,† respectively). Also, **HYR-1** can label other regions in wild type mice brain section (Fig. S5†), which means its specificity is extremely low. By comparison, the pyridyl-containing MFCs **HYR-14** and **HYR-16** exhibit appreciable amyloid plaque staining only at high concentrations (250–500 μM), suggesting that their Aβ binding affinity is somewhat reduced and thus these two compounds were not employed in radiolabeling studies (see below).

We have also probed the ability of the Cu^{2+} complexes of **HYR-4**, **-17** and **-18** to label the amyloid plaques in 5×FAD mice brain sections (Fig. 4). In this case, higher ligand to Congo Red ratios were used since the Cu^{2+} ions lead to some fluorescence quenching for our MFCs (Fig. S5 and S6†). However, the Cu^{2+} complexes of **HYR-4**, **-17** and **-18** can still label the amyloid plaques efficiently (Fig. 3), with the complexes of **HYR-4** and **-18**

MFC	Conc. (μM)	MFC : Congo Red ratio
HYR-1	25	5:1
HYR-4	25	5:1
HYR-14	500	100:1
HYR-16	250	50:1
HYR-17	25	5:1
HYR-18	25	5:1

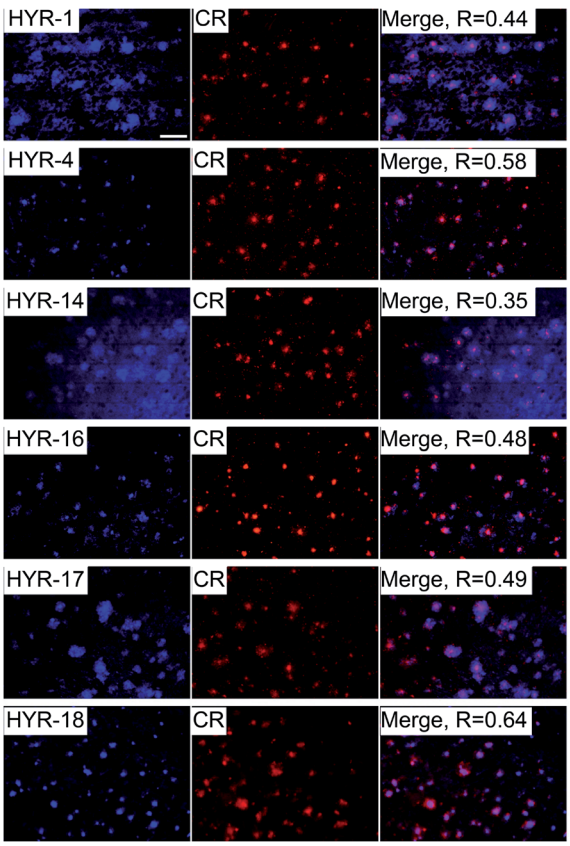

Fig. 3 Fluorescence microscopy images of 5×FAD mice brain sections incubated with multifunctional compounds **HYR-1**, **-4**, **-14**, **-16**, **-17** and **-18** (left panels), Congo Red (CR, middle panels), and merged images (right panels, with the Pearson's coefficient *R* shown). Scale bar: 100 μm. The concentration of MFC and MFC : Congo Red ratio used are listed at the top.

Cu complex	Conc. (μM)	Complex : CR ratio
Cu-HYR-4	50	10:1
Cu-HYR-17	50	10:1
Cu-HYR-18	50	10:1

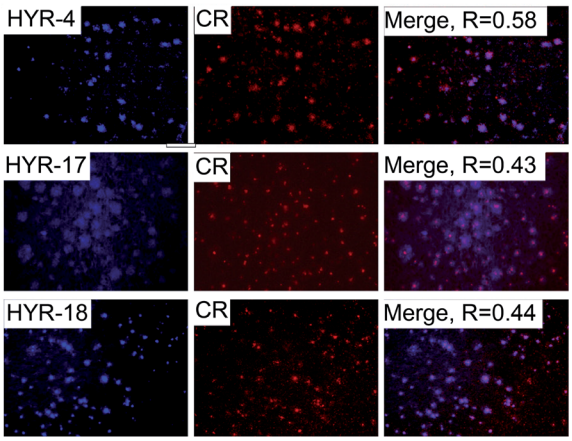

Fig. 4 Fluorescence microscopy images of 5×FAD mice brain sections incubated with Cu^{2+} complexes of **HYR-4**, **-17** and **-18** (left panels), Congo Red (middle panels), and merged images (right panels). Scale bar: 100 μm.

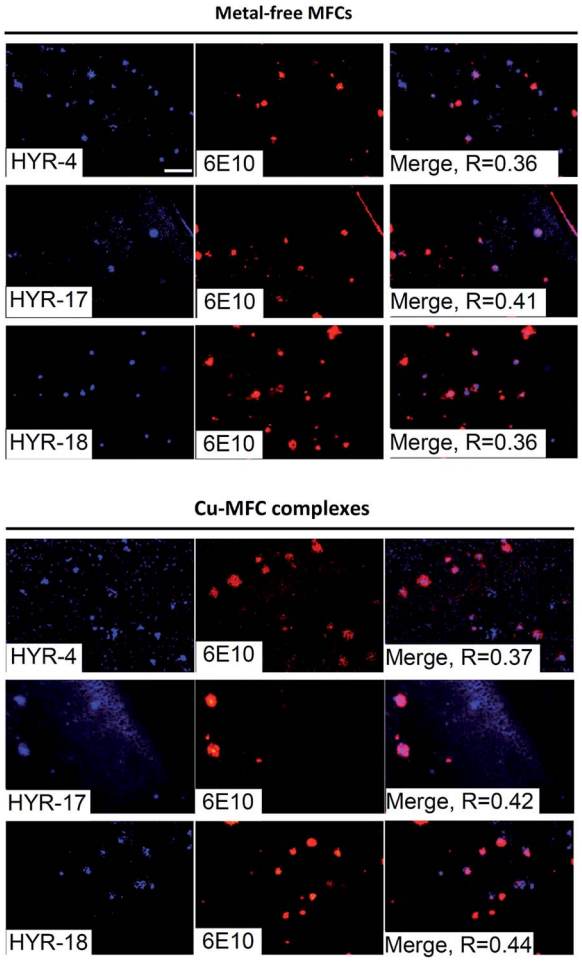

Fig. 5 Fluorescence microscopy images of 5×FAD mice brain sections incubated with MFCs **HYR-4**, **-17** and **-18** or their Cu(II) complexes (left panels), CF594-6E10 antibody (middle panels), and merged images (right panels). Scale bar: 100 μm.

showing higher specificity compared with the Cu-**HYR-17** complex. Finally, the fluorescently labeled CF594-6E10 antibody – which binds to a wide range of Aβ species, was employed to confirm that our MFCs and their Cu^{2+} complexes are able to specifically label the $A\beta_{42}$ species (Fig. 5). It is important to note that we have previously determined the stability constants for the Cu^{2+} complex of another 1,4,7-triazacyclononane-phenolate ligand, which was shown to bind Cu^{2+} very tightly.[49,50] Since the structural changes for the different MFCs described herein are remote from the Cu-binding site, we envision that the stability constants for the corresponding Cu^{2+} complexes will not vary significantly.

Modulation of metal-free and metal-induced Aβ aggregation

The ability of these MFCs to modulate the aggregation of $A\beta_{42}$ was then explored, both in the absence or presence of Cu^{2+} ions. The $A\beta_{42}$ peptide was used since it was shown to form neurotoxic soluble $A\beta_{42}$ oligomers.[12,13,18] Freshly prepared monomeric $A\beta_{42}$ solutions were treated with MFCs, Cu^{2+}, or both, and incubated for 24 hours at 37 °C, and the resulting samples were analysed by native gel electrophoresis/western blot analysis and transmission electron microscopy (TEM, Fig. 6). The former analysis method reveals the presence of smaller, soluble Aβ aggregates and their MW distribution, while the latter method

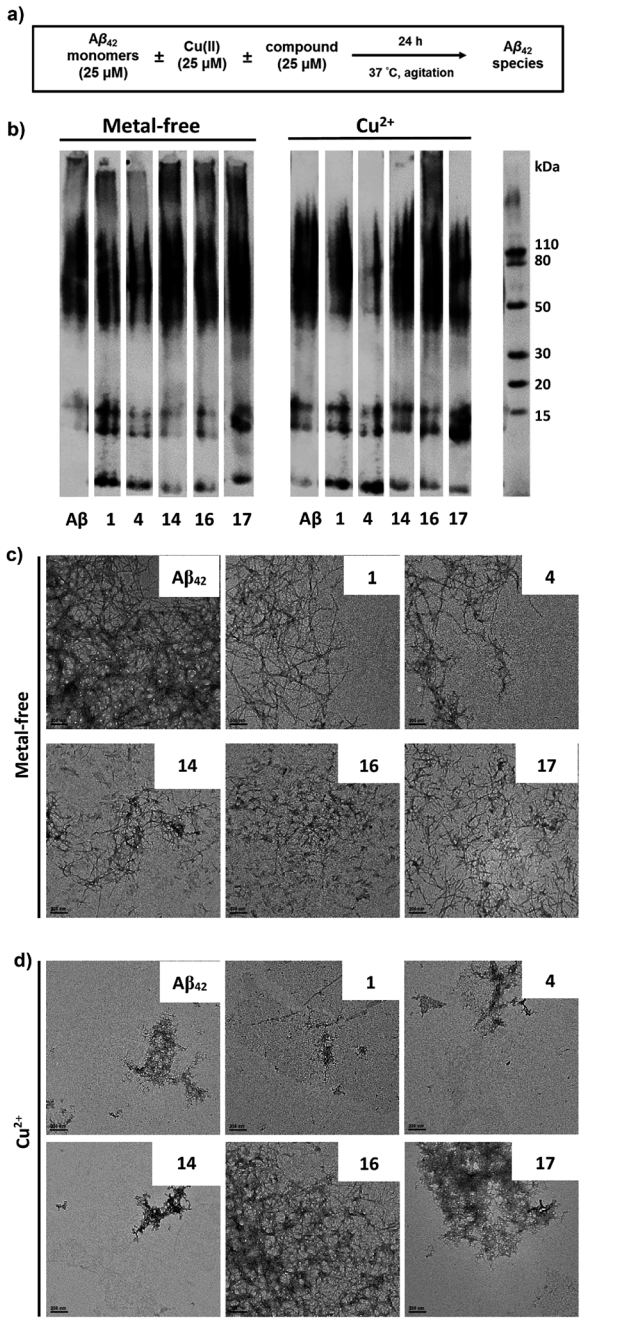

Fig. 6 Effects of the compounds on Cu^{2+}-free and Cu^{2+}-induced $A\beta_{42}$ aggregation. (a) Scheme of the inhibition experiment: freshly prepared $A\beta_{42}$ (25 μM) in the presence or absence of Cu^{2+} (25 μM) and with or without MFCs (25 μM) was incubated at 37 °C for 24 h with constant agitation. (b) Native gel/western blot analysis of the resulting $A\beta_{42}$ species using the 6E10 anti-Aβ antibody. (c) Representative TEM images of the $A\beta_{42}$ aggregates upon incubation with or without MFCs (scale bar, 200 nm). (d) Representative TEM images of the $A\beta_{42}$ aggregates upon incubation with Cu^{2+} and with or without MFCs (scale bar, 200 nm).

provides the characterization of the larger, insoluble Aβ aggregates that cannot penetrate the gel, and thus allowing us to visualize all $A\beta_{42}$ aggregates of various types and sizes.

While the aggregation of $A\beta_{42}$ in the absence of Cu^{2+} ions leads to well-defined $A\beta_{42}$ fibrils – as confirmed by TEM (Fig. 6c), the $A\beta_{42}$ aggregation in the presence of Cu^{2+} ions generates a limited amount of Aβ fibrils (Fig. 6d), and native gel/western blotting shows that the aggregation of $A\beta_{42}$ with Cu^{2+} ions yields mostly soluble $A\beta_{42}$ oligomers of various sizes (Fig. 6b). These results are consistent with our previous studies which suggest that Cu^{2+} can stabilize the soluble $A\beta_{42}$ oligomers and slow down the $A\beta_{42}$ aggregation.[33,59]

All MFCs **HYR-1**, **-4**, **-14**, **-16** and **-17** did not seem to significantly inhibit the $A\beta_{42}$ aggregation in the absence of Cu^{2+}, even though some morphological changes were observed for the $A\beta_{42}$ fibrils (Fig. 6b and c). Interestingly, the presence of **HYR-16** had a dramatic effect on the Cu^{2+}-mediated oligomerization of $A\beta_{42}$ and promoted the formation of larger $A\beta_{42}$ aggregates, as observed by TEM (Fig. 6d). Moreover, native gel/western blotting analysis reveals the presence of large, insoluble $A\beta_{42}$ aggregates at the top of the gel, which were not observed for the $A\beta_{42}$ aggregation in presence of only Cu^{2+} ions. Thus, **HYR-16** is expected to control the neurotoxicity of $A\beta_{42}$ species by accelerating the aggregation of toxic $A\beta_{42}$ oligomers into nontoxic $A\beta_{42}$ aggregates. By comparison, the other MFCs do not show a dramatic effect on Cu^{2+}-mediated $A\beta_{42}$ aggregation (Fig. 6b, left panels).

Cytotoxicity of MFCs and modulation of $A\beta_{42}$ neurotoxicity

The neurotoxicity of the MFCs and their ability to alleviate the Cu-induced $A\beta_{42}$ toxicity was performed using mouse neuroblastoma (N2a) cells. First, we examined the toxicity of all MFCs at various concentrations ranging from 2 to 20 μM (Fig. 7). Among the different MFCs, **HYR-4**, **-14** and **-16** exhibit no appreciable cell toxicity (>80% cell viability) up to 10 μM concentration, with **HYR-16** showing no cell toxicity up to 20 μM concentration, and thus these three MFCs were employed in $A\beta_{42}$-induced cytotoxicity studies. As we have shown before,[33,34] the presence of both Cu^{2+} ions and $A\beta_{42}$ leads to pronounced cell toxicity (~50% cell viability), likely due to the formation of neurotoxic $A\beta_{42}$ oligomers (Fig. 8). Interestingly, **HYR-16** can significantly alleviate the toxicity of Cu-stabilized $A\beta_{42}$ oligomers and increase the cell viability up to 80% *vs.* a 1% DMSO control, which is consistent with *in vitro* results that **HYR-16** can accelerate the aggregation of toxic $A\beta_{42}$ oligomers into nontoxic $A\beta_{42}$ aggregates. By comparison, **HYR-4** and **HYR-14** do not seem to significantly reduce the neurotoxicity of the Cu-$A\beta_{42}$ species (Fig. 8), suggesting that the 2-monomethylaminopyridyl fragment found in **HYR-16** is needed for the efficient alleviation of $A\beta_{42}$ oligomer neurotoxicity.

Antioxidant properties

Several previous reports have shown that the Cu^{2+} ions can interact with various Aβ species and lead to formation of reactive oxygen species (ROS) such as H_2O_2 and hydroxyl radicals ($OH^{\bullet}$).[31,60] In this regard, the antioxidant capacity of the pyridine derivatives **HYR-14** and **HYR-16** – the least toxic MFCs investigated herein, was first evaluated *via* the Trolox equivalent antioxidant capacity (TEAC) assay.[61] Both **HYR-14** and **HYR-16** showed better performance on scavenging the free radical $ABTS^{+\bullet}$ (ABTS = 2,2′-azino-bis(3-ethylbenzothiazoline-6-sulfonic acid)) than glutathione – a well-known antioxidant, at all the selected time points (1–15 min, Fig. 9a), with **HYR-16** showing an antioxidant capacity similar to Trolox.

In addition, the ability of **HYR-14** and **HYR-16** to quench the Cu-induced hydroxyl radical ($OH^{\bullet}$) generation was measured by using coumarin-3-carboxylic acid (CCA) antioxidant assay.[62] In this assay, the Cu^{2+} ions are reduced by ascorbic acid to Cu^{+} ions that then react with O_2 to produce $OH^{\bullet}$. The non-fluorescent

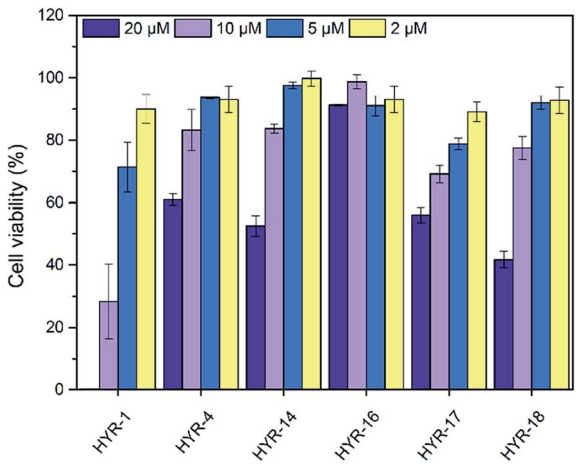

Fig. 7 Toxicity of MFCs at various concentrations in N2a cells, reported *vs.* a 1% DMSO control. The error bars indicate the standard deviations based on at least five samples per group.

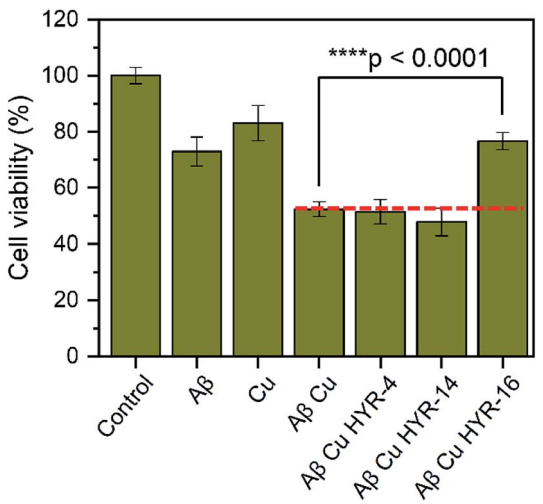

Fig. 8 The effect of MFCs on Cu^{2+}-induced $A\beta_{42}$ cytotoxicity, reported *vs.* a 1% DMSO control. N2a cells were treated with $A\beta_{42}$ (20 μM), $CuCl_2$ (20 μM), and MFCs (10 μM) and incubated for 40 h at 37 °C. The error bars indicate the standard deviations based on at least three samples per group, and the statistical analysis was evaluated according to one-way ANOVA (****$p < 0.0001$).

CCA reacts with OH˙ to produce the fluorescent 7-hydroxycoumarin-3-carboxylic acid (CCA-OH), and CCA-OH formation can be monitored to evaluate the efficacy of ligand binding to Cu and inhibition of OH˙ generation. At 80 μM, both of **HYR-14** and **HYR-16** show a strong Cu^{2+} binding affinity (corresponding to a 2 : 1 MFC : Cu ratio) and limit the generation of OH˙ (Fig. 9b and c), while **HYR-16** is able to limit the generation of OH˙ even at 40 μM (corresponding to a 1 : 1 MFC : Cu ratio). Overall, these studies reveal that **HYR-16** is the most potent anti-oxidant among the investigated MFCs, and along with its ability to efficiently destabilize the neurotoxic soluble $A\beta_{42}$ oligomers strongly suggest that **HYR-16** may potentially exhibit therapeutic properties in animal studies.

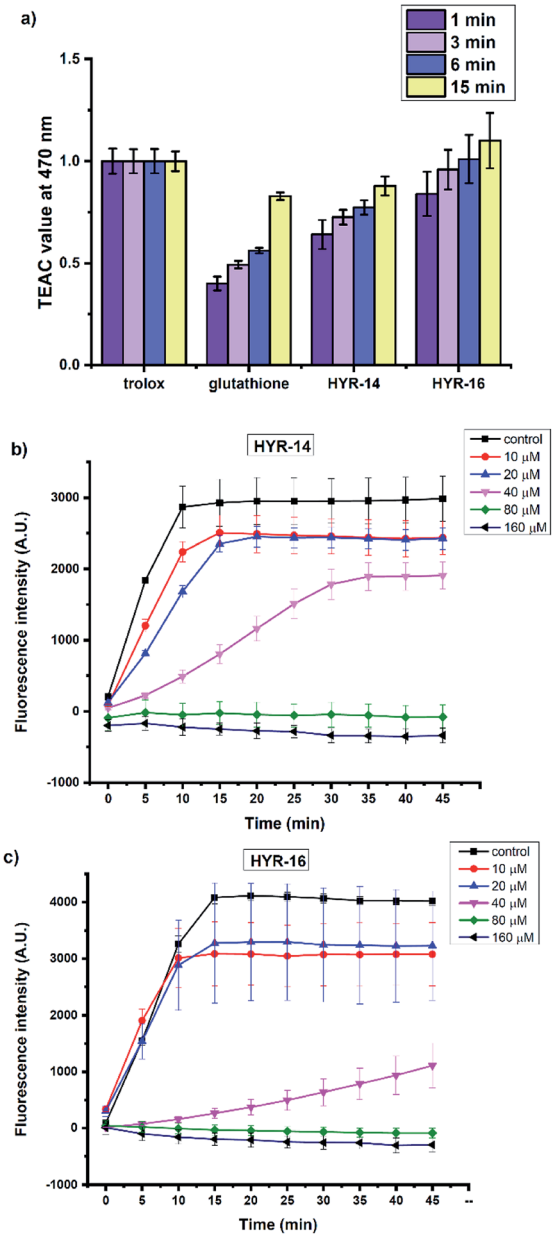

Fig. 9 (a) The antioxidant activity of Trolox, glutathione, **HYR-14**, and **HYR-16** (25–100 μM) at 1, 3, 6, and 15 minutes assessed by TEAC assay. The TEAC values of glutathione, **HYR-14**, and **HYR-16** were normalized to the Trolox activity. The inhibitory activity of (b) **HYR-14** and (c) **HYR-16** toward Cu-mediated hydroxyl radical generation, evaluated *via* the CCA antioxidant assay. Conditions: [CCA] = 100 μM; [$CuSO_4$] = 40 μM; [ascorbic acid] = 400 μM; [**HYR-14**/**HYR-16**] = 0–160 μM; λ_{ex} = 395 nm; λ_{ex} = 450 nm. All experiments were performed in triplicate and the error bars indicate the standard deviation for each measurement.

Table 1 Molecular weights for MFCs and log D_{oct} values for the corresponding ^{64}Cu-labeled complexes

Ligand	MW (g mol^{-1})	log D_{oct}
HYR-1	439.6	1.08 ± 0.11
HYR-4	425.6	1.29 ± 0.19
HYR-14	440.6	0.58 ± 0.05
HYR-16	426.6	0.56 ± 0.17
HYR-17	439.6	1.30 ± 0.15
HYR-18	679.9	1.09 ± 0.11

Radiolabeling and log D_{oct} value determination

One crucial factor for developing imaging agents for neurodegenerative diseases is that they should be able to effectively cross the blood–brain barrier (BBB). To determine the hydrophobicity of the radiolabeled compounds, the octanol/PBS partition coefficient values log D_{oct} were determined for the ^{64}Cu complexes of **HYR-1**, **-4**, **-14**, **-16**, **-17** and **-18**. The obtained log D_{oct} values for the ^{64}Cu-radiolabeled complexes **HYR-1**, **-4**, **-17** and **-18** are in the range of 1.08–1.30 (Table 1), which supports their potential ability to cross the BBB, since log D values between 0.9 and 2.5 are considered optimal.[63] In contrast, the ^{64}Cu complexes of **HYR-14** and **-16** exhibit log D_{oct} values of ~0.6, suggesting that 2-pyridyl-benzothiazole derivatives may be too hydrophilic to cross the BBB. Thus, only the MFCs **HYR-1**, **-4**, **-17** and **-18** were employed in the subsequent radiochemistry studies.

Ex vivo autoradiography studies

Ex vivo autoradiography studies using brain sections of transgenic 5×FAD mice were also performed to determine the

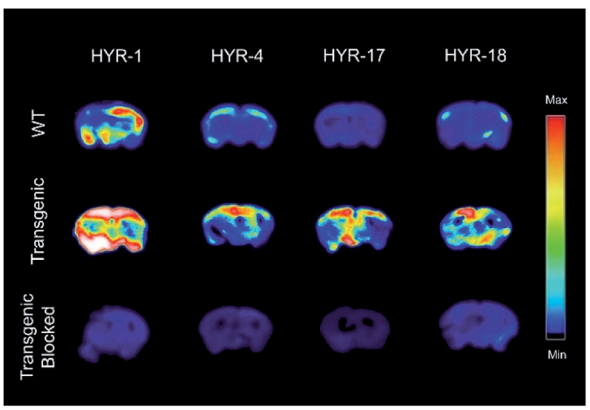

Fig. 10 Autoradiography images of 5×FAD mice brain sections with the absence and presence with a known Aβ blocking agent (B_1).

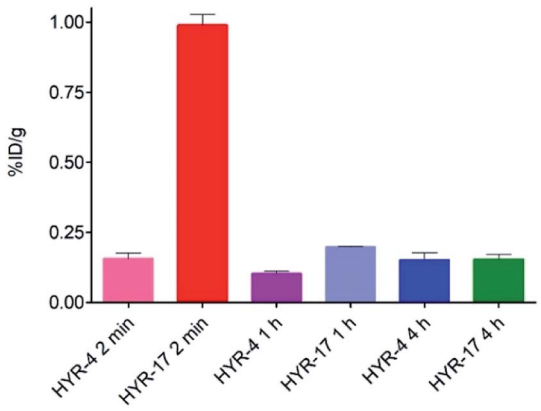

Fig. 11 Brain uptake (% injected dose per gram, %ID per g) results from the biodistribution studies in CD-1 mice, at 2, 60, and 240 min post injection.

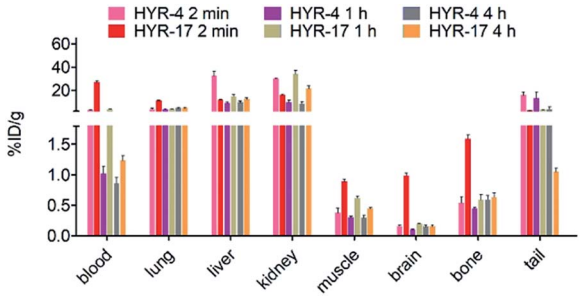

Fig. 12 Various organs uptake (%ID per g) of ^{64}Cu-labeled **HYR-4** and **HYR-17** from the biodistribution studies in CD-1 mice, at 2, 60, and 240 min post injection.

specific binding to the amyloid plaques of the ^{64}Cu-labeled **HYR-1**, **-4**, **-17** and **-18**. The brain sections were stained, washed, and radioimaged as described in the experimental section. When compared with WT brain sections that show a limited background intensity (Fig. 10, first row), the ^{64}Cu-labeled complexes of **HYR-4**, **-17** and **-18** show an increased autoradiography intensity for the 5×FAD mouse brain sections (Fig. 10, second row). The ^{64}Cu-labeled **HYR-1** also exhibits non-specific binding as appreciable autoradiography intensity is observed for WT brain sections, which is consistent with the brain section fluorescent imaging studies described above. Finally, the specific binding to amyloid plaques of the ^{64}Cu-labeled MFCs was confirmed by blocking with the non-radioactive blocking agent B_1 (Fig. S6†), which led to a markedly decreased autoradiography intensity (Fig. 10, third row). Overall, these autoradiography results strongly suggest that the ^{64}Cu-labeled MFCs **HYR-4**, **-17** and **-18** have the necessary amyloid-binding specificity to be used as imaging agents *in vivo*. The MFC **HYR-18**, the bis-(2-phenylbenzothiazole) analogue of **HYR-4**, exhibits a slightly lower log D_{oct} value than **HYR-4**, and it was also perceived to have a too large MW for an efficient brain uptake. Since **HYR-4** already exhibits a promising log D_{oct} value and specific binding to amyloid plaques, we decided to not include **HYR-18** in the *in vivo* biodistribution studies.

Biodistribution studies

Encouraged by the promising *in vitro* radiolabeling and amyloid-binding studies, *in vivo* biodistribution experiments were performed to probe the uptake of ^{64}Cu-labelled **HYR-4** and **-17** complexes using normal CD-1 mice. The retention and accumulation of the ^{64}Cu-labeled complexes in selected organs was evaluated at 2, 60, and 240 minutes after tracer administration. Excitingly, ^{64}Cu-**HYR-17** shows an appreciable brain uptake of 0.99 ± 0.04 % injected dose per gram (%ID per g) at 2 min post injection, which drops to 0.20 ± 0.01 %ID per g at 60 min (Fig. 11 and Table 2). By comparison, ^{64}Cu-**HYR-4** shows a relatively low brain uptake of 0.16 ± 0.02 %ID per g at 2 min post injection, although ^{64}Cu-**HYR-4** shows a similar blood uptake to that of ^{64}Cu-**HYR-17** (Fig. 12), and suggesting that the structure of **HYR-17** containing the 4-hydroxyl substituent and tacn azamacrocycle connected to the 5 position of the benzothiazole ring should lead to improved brain uptake properties for the corresponding ^{64}Cu-labeled complexes. Overall, these biodistribution studies strongly suggest that the ^{64}Cu-**HYR-17** complex can efficiently cross the BBB and thus could serve as a PET imaging agent for the detection of Aβ aggregates *in vivo*. Importantly, the rapid clearance from the brain of WT mice suggest that these radiolabeled MFCs do not release ^{64}Cu in the brain to an appreciable extent, and thus should not lead to a significant background PET signal in WT or healthy controls.

Table 2 Overall biodistribution results of ^{64}Cu-Labeled **HYR-4** and **HYR-17** for the three time points evaluated (2, 60, and 240 min; % injected dose/gram, mean ± SEM)

	HYR-4			**HYR-17**		
Organ	2 min	60 min	240 min	2 min	60 min	240 min
Blood	2.85 ± 0.52	1.02 ± 0.12	0.86 ± 0.10	26.82 ± 1.59	3.70 ± 0.06	1.24 ± 0.08
Lung	3.77 ± 0.88	3.36 ± 0.25	4.47 ± 0.49	11.02 ± 0.52	3.65 ± 0.16	4.47 ± 0.49
Liver	32.48 ± 3.94	8.84 ± 0.98	9.57 ± 1.19	11.50 ± 0.69	14.79 ± 1.71	12.16 ± 1.28
Kidney	30.27 ± 0.44	9.39 ± 2.02	8.24 ± 1.95	15.96 ± 0.81	34.17 ± 2.87	21.40 ± 2.27
Muscle	0.37 ± 0.08	0.30 ± 0.02	0.30 ± 0.04	0.89 ± 0.04	0.62 ± 0.02	0.45 ± 0.01
Brain	**0.16 ± 0.02**	**0.10 ± 0.01**	**0.15 ± 0.03**	**0.99 ± 0.04**	**0.20 ± 0.00**	**0.15 ± 0.02**
Bone	0.54 ± 0.11	0.45 ± 0.01	0.59 ± 0.07	1.59 ± 0.07	0.59 ± 0.09	0.64 ± 0.07
Tail	15.91 ± 2.84	12.8 ± 5.38	3.69 ± 1.92	2.53 ± 0.16	3.20 ± 0.29	1.05 ± 0.05

Conclusions

Herein we report several metal-chelating benzothiazole multifunctional compounds (MFCs) and investigate their various biochemical, *in vitro*, and *in vivo* properties to bind to various Aβ species, modulate Aβ aggregation and its neurotoxicity, and potentially act as ^{64}Cu PET imaging agents for *in vivo* detection of Aβ aggregates. During these studies, we have obtained important structure–activity relationships (SAR) that will guide us to develop improved MFCs as potential therapeutic or diagnostic agents for AD. Firstly, when comparing **HYR-4** *vs.* **HYR-1** and **HYR-16** *vs.* **HYR-14**, we can conclude that the compounds containing a monomethylamino *vs.* a dimethylamino group exhibit an increased specificity for the Aβ aggregates as well as reduced cytotoxicity. Secondly, the introduction of a pyridyl group in MFCs such as **HYR-14** and **HYR-16** dramatically reduces their cytotoxicity and improves their antioxidant properties. Taken together, the MFC **HYR-16** containing the 2-monomethylamino-pyridyl fragment is most effective at alleviating the $A\beta_{42}$ oligomer neurotoxicity and modulating Aβ aggregation. Thirdly, all investigated MFCs can be efficiently radiolabeled with the ^{64}Cu radioisotope, and the ^{64}Cu complexes of **HYR-4**, **HYR-17**, and **HYR-18** exhibit acceptable lipophilicity and specific radiolabeling of amyloid plaques *ex vivo*.

Interestingly, the position of the hydroxyl group and the metal-chelating tacn azamacrocycle on the benzothiazole ring has a dramatic effect on the BBB permeability of these ^{64}Cu-labelled MFCs: the ^{64}Cu complex of **HYR-17** – which contains the 4-hydroxyl substituent and tacn azamacrocycle connected to the 5 position of the benzothiazole ring, exhibits the highest brain uptake. Finally, our results suggest that employing **HYR-18**, the bis-(2-phenylbenzothiazole) analogue of **HYR-4**, does not improve the lipophilicity or specificity for amyloid plaques, while unnecessarily increasing the MW and thus possibly limiting its BBB permeability.

Overall, these detailed studies suggest that **HYR-16** is the most effective MFC at alleviating the neurotoxicity of soluble Aβ oligomers, and thus it lends promise to the use of **HYR-16** and its second-generation derivatives in future animal studies to evaluate their therapeutic properties. Moreover, **HYR-17** exhibits the largest brain uptake and *ex vivo* specificity for native amyloid plaques, and derivatives of this MFC with similar positioning of the benzothiazole ring substituents will be used as lead compounds for microPET imaging studies in WT *vs.* AD transgenic mice, toward the development of improved ^{64}Cu PET imaging agents for AD diagnosis.

Ethical statement

All animal studies were performed in strict accordance with the NIH guidelines for the care and use of laboratory animals (NIH Publication No. 85-23 Rev. 1985) and were in compliance with the Guidelines for Care and Use of Research Animals established by the Division of Comparative Medicine and the Animal Studies Committee of Washington University in St. Louis. The animal protocol #20190073 including all the animal studies performed herein was reviewed and approved by the Institutional Animal Care and Use Committee of Washington University in St. Louis.

Conflicts of interest

There are no conflicts to declare.

Acknowledgements

L. M. M. acknowledges research funding from NIH (R01GM114588), the Alzheimer's Association (NIRG 12-259199), and the Washington University Knight Alzheimer's Disease Research Center (NIH P50AG05681). The authors would like to thank the small animal imaging facility at Washington University School of Medicine for excellent technical assistance, Cedric Mpoy for valuable assistance with animal studies, and the Isotope Production Group at Washington University for on time weekly production of ^{64}Cu.

Notes and references

1 K. P. Kepp, *Chem. Rev.*, 2012, **112**, 5193–5239.
2 Alzheimer's Association, *Alzheimer's Dementia*, 2019, vol. 15, pp. 321–387.
3 P. Sweeney, H. Park, M. Baumann, J. Dunlop, J. Frydman, R. Kopito, A. McCampbell, G. Leblanc, A. Venkateswaran, A. Nurmi and R. Hodgson, *Transl. Neurodegener.*, 2017, **6**, 6.
4 M. Citron, *Nat. Rev. Drug Discovery*, 2010, **9**, 387–398.
5 F. M. LaFerla, K. N. Green and S. Oddo, *Nat. Rev. Neurosci.*, 2007, **8**, 499–509.
6 E. Karran, M. Mercken and B. D. Strooper, *Nat. Rev. Drug Discovery*, 2011, **10**, 698–712.
7 F. Chiti and C. M. Dobson, *Annu. Rev. Biochem.*, 2017, **86**, 27–68.
8 M. P. Mattson, *Nature*, 2004, **430**, 631–639.
9 E. McGowan, F. Pickford, J. Kim, L. Onstead, J. Eriksen, C. Yu, L. Skipper, M. P. Murphy, J. Beard, P. Das, K. Jansen, M. DeLucia, W. L. Lin, G. Dolios, R. Wang, C. B. Eckman, D. W. Dickson, M. Hutton, J. Hardy and T. Golde, *Neuron*, 2005, **47**, 191–199.
10 J. Kim, L. Onstead, S. Randle, R. Price, L. Smithson, C. Zwizinski, D. W. Dickson, T. Golde and E. McGowan, *J. Neurosci.*, 2007, **27**, 627–633.
11 I. Kuperstein, K. Broersen, I. Benilova, J. Rozenski, W. Jonckheere, M. Debulpaep, A. Vandersteen, I. Segers-Nolten, K. Van Der Werf, V. Subramaniam, D. Braeken, G. Callewaert, C. Bartic, R. D'Hooge, I. C. Martins, F. Rousseau, J. Schymkowitz and B. De Strooper, *EMBO J.*, 2010, **29**, 3408–3420.
12 K. Pauwels, T. L. Williams, K. L. Morris, W. Jonckheere, A. Vandersteen, G. Kelly, J. Schymkowitz, F. Rousseau, A. Pastore, L. C. Serpell and K. Broersen, *J. Biol. Chem.*, 2012, **287**, 5650–5660.

13 Y. S. Gong, L. Chang, K. L. Viola, P. N. Lacor, M. P. Lambert, C. E. Finch, G. A. Krafft and W. L. Klein, *Proc. Natl. Acad. Sci. U. S. A.*, 2003, **100**, 10417–10422.
14 W. L. Klein, G. A. Krafft and C. E. Finch, *Trends Neurosci.*, 2001, **24**, 219–224.
15 M. P. Lambert, A. K. Barlow, B. A. Chromy, C. Edwards, R. Freed, M. Liosatos, T. E. Morgan, I. Rozovsky, B. Trommer, K. L. Viola, P. Wals, C. Zhang, C. E. Finch, G. A. Krafft and W. L. Klein, *Proc. Natl. Acad. Sci. U. S. A.*, 1998, **95**, 6448–6453.
16 A. I. Bush, *Curr. Opin. Chem. Biol.*, 2000, **4**, 184–191.
17 I. Benilova, E. Karran and B. De Strooper, *Nat. Neurosci.*, 2012, **15**, 349–357.
18 S. J. C. Lee, E. Nam, H. J. Lee, M. G. Savelieff and M. H. Lim, *Chem. Soc. Rev.*, 2017, **46**, 310–323.
19 M. D. Kirkitadze, G. Bitan and D. B. Teplow, *J. Neurosci. Res.*, 2002, **69**, 567–577.
20 J. W. Um, H. B. Nygaard, J. K. Heiss, M. A. Kostylev, M. Stagi, A. Vortmeyer, T. Wisniewski, E. C. Gunther and S. M. Strittmatter, *Nat. Neurosci.*, 2012, **15**, 1227–U1285.
21 T. Umeda, T. Tomiyama, N. Sakama, S. Tanaka, M. P. Lambert, W. L. Klein and H. Mori, *J. Neurosci. Res.*, 2011, **89**, 1031–1042.
22 S. Lesne, M. T. Koh, L. Kotilinek, R. Kayed, C. G. Glabe, A. Yang, M. Gallagher and K. H. Ashe, *Nature*, 2006, **440**, 352–357.
23 D. M. Walsh and D. J. Selkoe, *J. Neurochem.*, 2007, **101**, 1172–1184.
24 M. A. Lovell, J. D. Robertson, W. J. Teesdale, J. L. Campbell and W. R. Markesbery, *J. Neurol. Sci.*, 1998, **158**, 47–52.
25 K. J. Barnham, C. L. Masters and A. I. Bush, *Nat. Rev. Drug Discovery*, 2004, **3**, 205–214.
26 H. Kozlowski, A. Janicka-Klos, J. Brasun, E. Gaggelli, D. Valensin and G. Valensin, *Coord. Chem. Rev.*, 2009, **253**, 2665–2685.
27 P. Faller, *ChemBioChem*, 2009, **10**, 2837–2845.
28 P. Faller and C. Hureau, *Dalton Trans.*, 2009, 1080–1094.
29 P. Faller, C. Hureau and G. La Penna, *Acc. Chem. Res.*, 2014, **47**, 2252–2259.
30 L. E. Scott and C. Orvig, *Chem. Rev.*, 2009, **109**, 4885–4910.
31 C. Hureau and P. Faller, *Biochimie*, 2009, **91**, 1212–1217.
32 C. Cheignon, M. Tomas, D. Bonnefont-Rousselot, P. Faller, C. Hureau and F. Collin, *Redox Biol.*, 2018, **14**, 450–464.
33 A. K. Sharma, S. T. Pavlova, J. Kim, D. Finkelstein, N. J. Hawco, N. P. Rath, J. Kim and L. M. Mirica, *J. Am. Chem. Soc.*, 2012, **134**, 6625–6636.
34 A. K. Sharma, S. T. Pavlova, J. Kim, J. Kim and L. M. Mirica, *Metallomics*, 2013, **5**, 1529–1536.
35 M. G. Savelieff, A. S. DeToma, J. S. Derrick and M. H. Lim, *Acc. Chem. Res.*, 2014, **47**, 2475–2482.
36 L. M. F. Gomes, A. Mahammed, K. E. Prosser, J. R. Smith, M. A. Silverman, C. J. Walsby, Z. Gross and T. Storr, *Chem. Sci.*, 2019, **10**, 1634–1643.
37 S. Ayala, P. Genevaux, C. Hureau and P. Faller, *ACS Chem. Neurosci.*, 2019, **10**, 3366–3374.
38 M. G. Savelieff, G. Nam, J. Kang, H. J. Lee, M. Lee and M. H. Lim, *Chem. Rev.*, 2019, **119**, 1221–1322.
39 W. E. Klunk, H. Engler, A. Nordberg, Y. M. Wang, G. Blomqvist, D. P. Holt, M. Bergstrom, I. Savitcheva, G. F. Huang, S. Estrada, B. Ausen, M. L. Debnath, J. Barletta, J. C. Price, J. Sandell, B. J. Lopresti, A. Wall, P. Koivisto, G. Antoni, C. A. Mathis and B. Langstrom, *Ann. Neurol.*, 2004, **55**, 306–319.
40 A. Nordberg, *Curr. Opin. Neurol.*, 2007, **20**, 398–402.
41 H. A. Archer, P. Edison, D. J. Brooks, J. Barnes, C. Frost, T. Yeatman, N. C. Fox and M. N. Rossor, *Ann. Neurol.*, 2006, **60**, 145–147.
42 S. R. Choi, G. Golding, Z. Zhuang, W. Zhang, N. Lim, F. Hefti, T. E. Benedum, M. R. Kilbourn, D. Skovronsky and H. F. Kung, *J. Nucl. Med.*, 2009, **50**, 1887–1894.
43 H. F. Kung, S. R. Choi, W. Qu, W. Zhang and D. Skovronsky, *J. Med. Chem.*, 2009, **53**, 933–941.
44 M. A. Mintun, G. N. LaRossa, Y. I. Sheline, C. S. Dence, S. Y. Lee, R. H. Mach, W. E. Klunk, C. A. Mathis, S. T. DeKosky and J. C. Morris, *Neurology*, 2006, **67**, 446–452.
45 K. Serdons, C. Terwinghe, P. Vermaelen, K. Van Laere, H. Kung, L. Mortelmans, G. Bormans and A. Verbruggen, *J. Med. Chem.*, 2009, **52**, 1428–1437.
46 J. L. Hickey, S. Lim, D. J. Hayne, B. M. Paterson, J. M. White, V. L. Villemagne, P. Roselt, D. Binns, C. Cullinane, C. M. Jeffery, R. I. Price, K. J. Barnham and P. S. Donnelly, *J. Am. Chem. Soc.*, 2013, **135**, 16120–16132.
47 M. Roger, L. M. P. Lima, M. Frindel, C. Platas-Iglesias, J.-F. Gestin, R. Delgado, V. Patinec and R. Tripier, *Inorg. Chem.*, 2013, **52**, 5246–5259.
48 A. K. Sharma, J. Kim, J. T. Prior, N. J. Hawco, N. P. Rath, J. Kim and L. M. Mirica, *Inorg. Chem.*, 2014, **53**, 11367–11376.
49 N. Bandara, A. K. Sharma, S. Krieger, J. W. Schultz, B. H. Han, B. E. Rogers and L. M. Mirica, *J. Am. Chem. Soc.*, 2017, **139**, 12550–12558.
50 A. K. Sharma, J. W. Schultz, J. T. Prior, N. P. Rath and L. M. Mirica, *Inorg. Chem.*, 2017, **56**, 13801–13814.
51 S. R. Choi, J. A. Schneider, D. A. Bennett, T. G. Beach, B. J. Bedell, S. P. Zehntner, M. J. Krautkramer, H. F. Kung, D. M. Skovronsky, F. Hefti and C. M. Clark, *Alzheimer Dis. Assoc. Disord.*, 2012, **26**, 8–16.
52 E. Arturoni, C. Bazzicalupi, A. Bencini, C. Caltagirone, A. Danesi, A. Garau, C. Giorgi, V. Lippolis and B. Valtancoli, *Inorg. Chem.*, 2008, **47**, 6551–6563.
53 M. Roger, L. M. Lima, M. Frindel, C. Platas-Iglesias, J.-F. o. Gestin, R. Delgado, V. r. Patinec and R. l. Tripier, *Inorg. Chem.*, 2013, **52**, 5246–5259.
54 E. M. Snyder, D. Asik, S. M. Abozeid, A. Burgio, G. Bateman, S. G. Turowski, J. A. Spernyak and J. R. Morrow, *Angew. Chem., Int. Ed.*, 2020, **132**, 2435–2440.
55 K. Serdons, T. Verduyckt, D. Vanderghinste, P. Borghgraef, J. Cleynhens, F. Van Leuven, H. Kung, G. Bormans and A. Verbruggen, *Eur. J. Med. Chem.*, 2009, **44**, 1415–1426.
56 W. E. Klunk, Y. Wang, G.-f. Huang, M. L. Debnath, D. P. Holt and C. A. Mathis, *Life Sci.*, 2001, **69**, 1471–1484.

57 A. Lockhart, L. Ye, D. B. Judd, A. T. Merritt, P. N. Lowe, J. L. Morgenstern, G. Z. Hong, A. D. Gee and J. Brown, *J. Biol. Chem.*, 2005, **280**, 7677–7684.
58 H. Oakley, S. L. Cole, S. Logan, E. Maus, P. Shao, J. Craft, A. Guillozet-Bongaarts, M. Ohno, J. Disterhoft, L. Van Eldik, R. Berry and R. Vassar, *J. Neurosci.*, 2006, **26**, 10129–10140.
59 Y. Zhang, D. L. Rempel, J. Zhang, A. K. Sharma, L. M. Mirica and M. L. Gross, *Proc. Natl. Acad. Sci. U. S. A.*, 2013, **110**, 14604–14609.
60 M. A. Smith, P. L. Harris, L. M. Sayre and G. Perry, *Proc. Natl. Acad. Sci. U. S. A.*, 1997, **94**, 9866–9868.
61 R. Re, N. Pellegrini, A. Proteggente, A. Pannala, M. Yang and C. Rice-Evans, *Free Radical Biol. Med.*, 1999, **26**, 1231–1237.
62 Y. Manevich, K. D. Held and J. E. Biaglow, *Radiat. Res.*, 1997, **148**, 580–591.
63 D. D. Dischino, M. J. Welch, M. R. Kilbourn and M. E. Raichle, *J. Nucl. Med.*, 1983, **24**, 1030–1038.